

Supporting Information

for

Pillar[5]arene-Based Supramolecular Plasmonic Thin Films for Label-free, Quantitative and Multiplex SERS Detection

Verónica Montes-García,[†] Borja-Gómez,[‡] Diego Martínez-Solís,[§] José M. Taboada,^{||} Norman Jiménez-Otero,[⊥] Jacobo de Uña-Álvarez,[⊥] Fernando Obelleiro,[§] Luis García-Río,[‡] Jorge Pérez-Juste,^{*,†} Isabel Pastoriza-Santos^{*,†}

[†] Departamento de Química Física y CINBIO, Universidade de Vigo, 36310 Vigo, Spain

[‡] Centro Singular de Investigación en Química Biológica y Materiales Moleculares (CIQUS), Departamento de Química Física, Universidad de Santiago, 15782 Santiago, Spain.

[§] Departamento de Teoría de la Señal y Comunicaciones, Universidade de Vigo, 36310 Vigo, Spain

^{||} Departamento Tecnología de los Computadores y de las Comunicaciones, Universidad de Extremadura, 10003 Cáceres, Spain

[⊥] Departamento de Estadística e Investigación Operativa, Facultad de Ciencias Económicas y Empresariales & CINBIO, Universidade de Vigo, 36310 Vigo, Spain

* juste@uvigo.es and pastoriza@uvigo.es

Pages S-1 through S-18

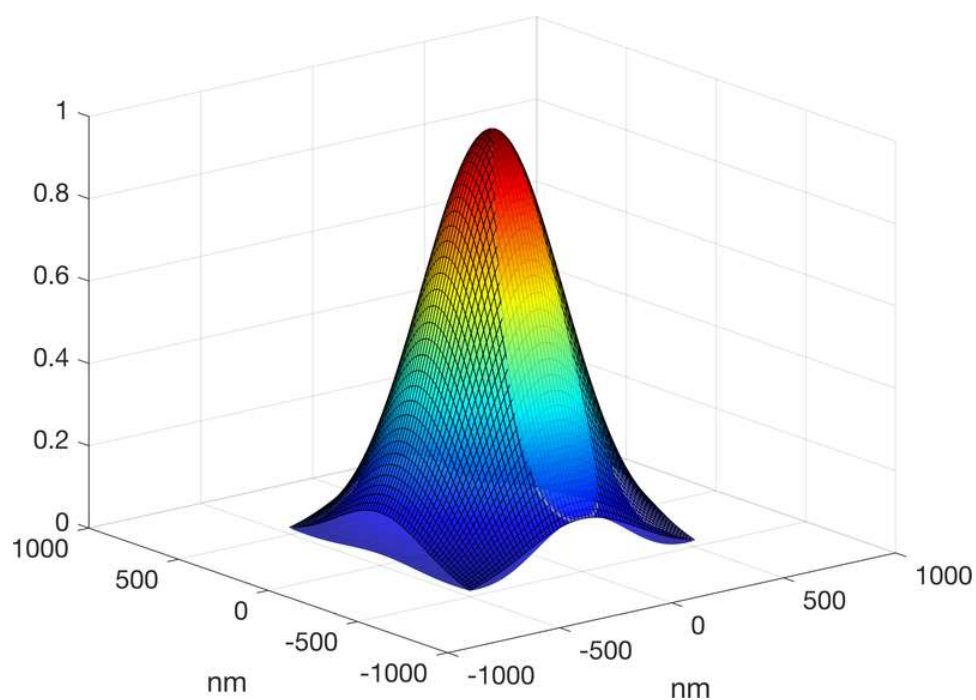


Figure S1. 2D Gaussian profile used to weight simulated SERS (gridded surface) and Gaussian beam with N.A. = 0.75 (color surface).

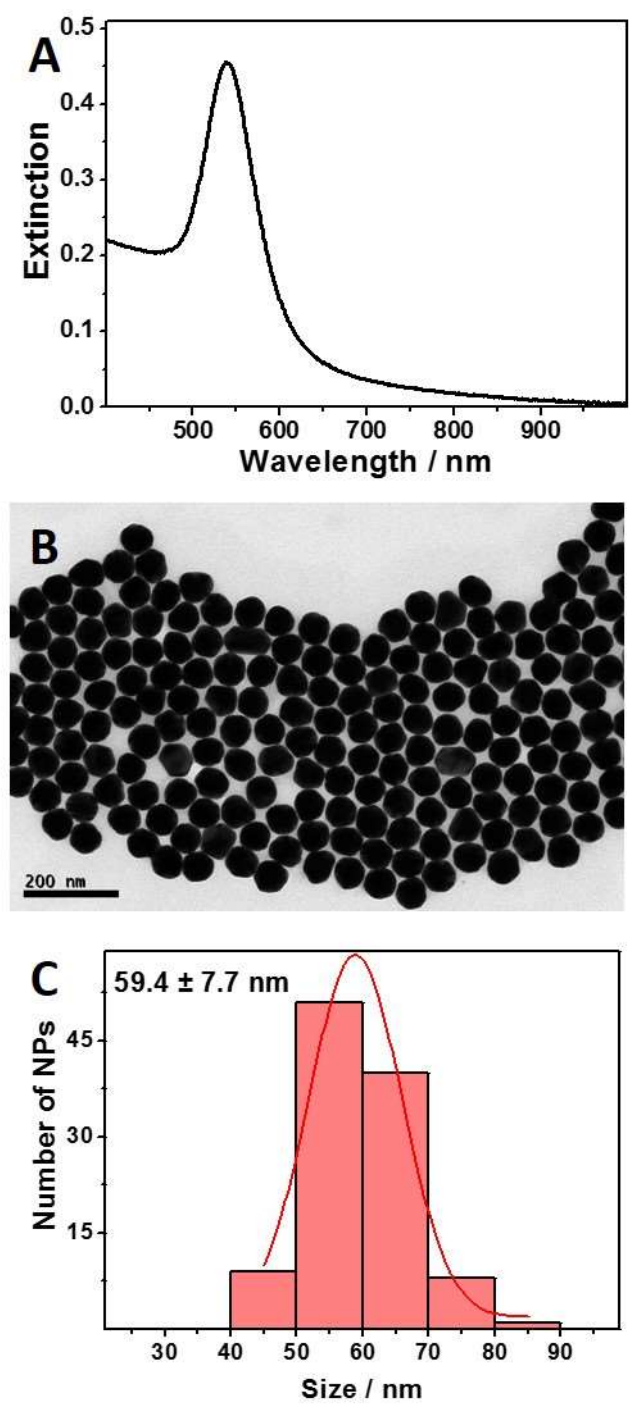


Figure S2. (A) Visible-NIR extinction spectrum of citrate-stabilized Au nanoparticles in water. (B) Representative TEM image. (C) Size distribution histogram obtained from TEM analysis.

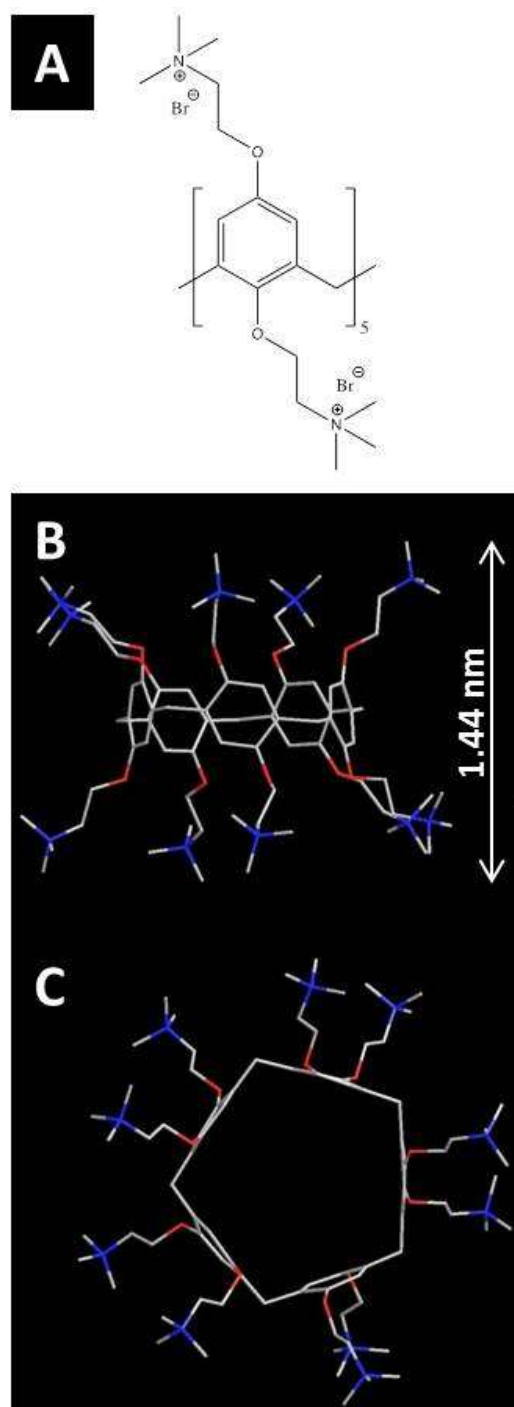


Figure S3. (A-C) Chemical structure of pillar[5]arene. (B) Side view and (C) upper view.

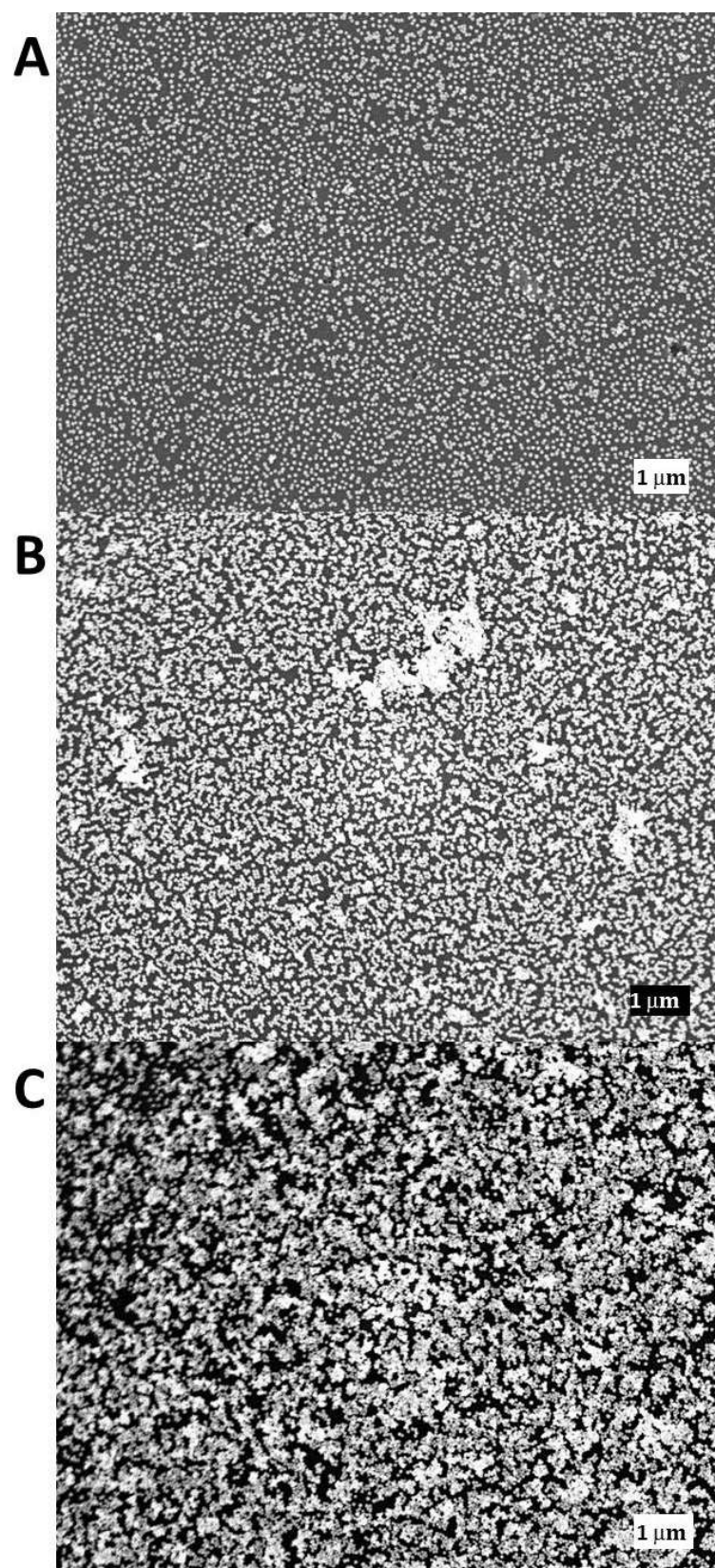


Figure S4. SEM images of AuNP-AP[5]A assemblies on positively charged PDDA modified glass obtained after different AuNP-AP[5]A depositions cycles: one **(A)**, two **(B)** and three **(C)**.

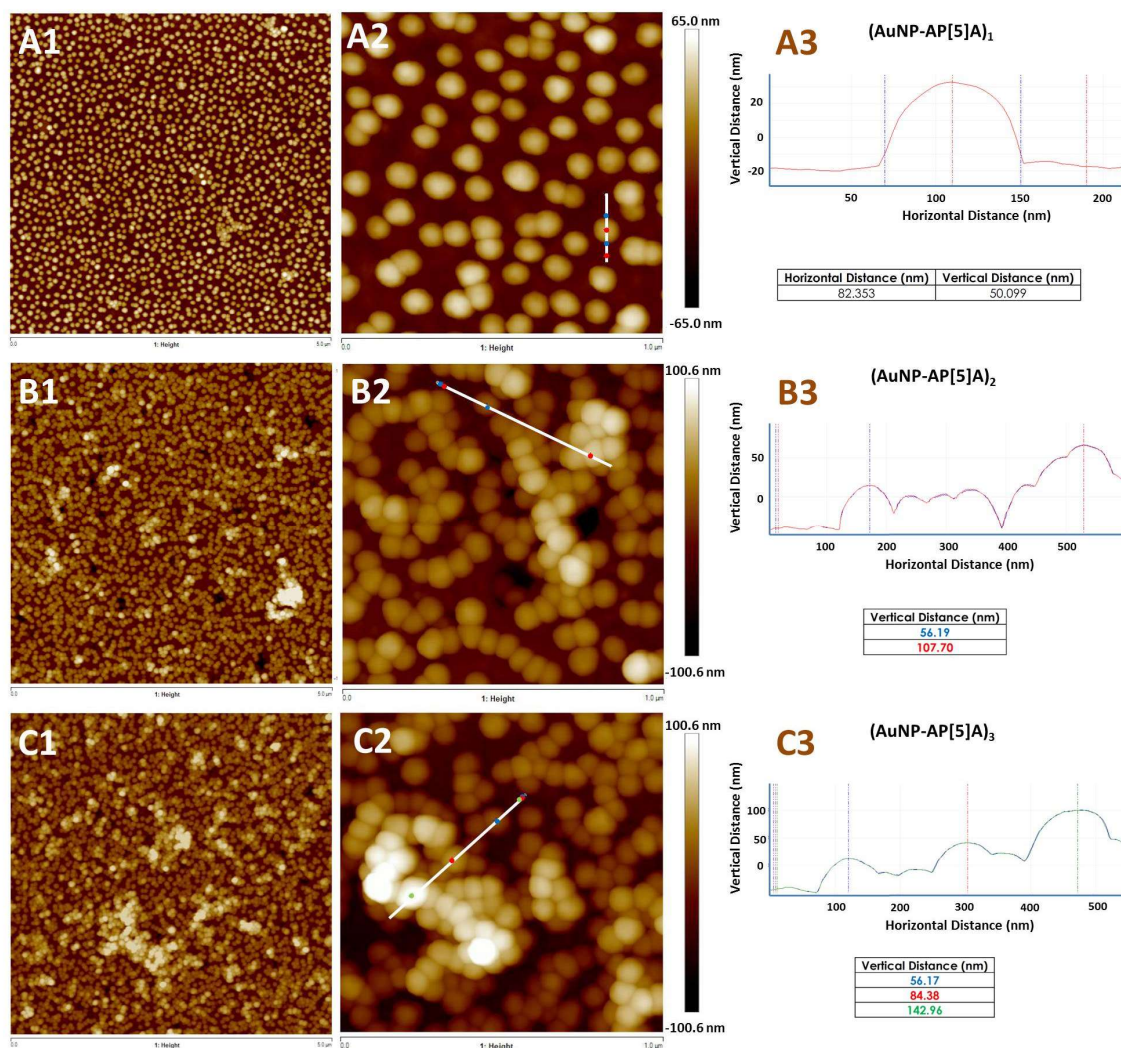


Figure S5. AFM topography images of the plasmonic substrates with one **(A)**, two **(B)** and three **(C)** AuNP-AP[5]A deposition cycles; namely (AuNP-AP[5]A)₁, (AuNP-AP[5]A)₂ and (AuNP-AP[5]A)₃, respectively. The plots in A3, B3 and C3 are cross sections of lines marked in the topography images of A2, B2 and C2, respectively.

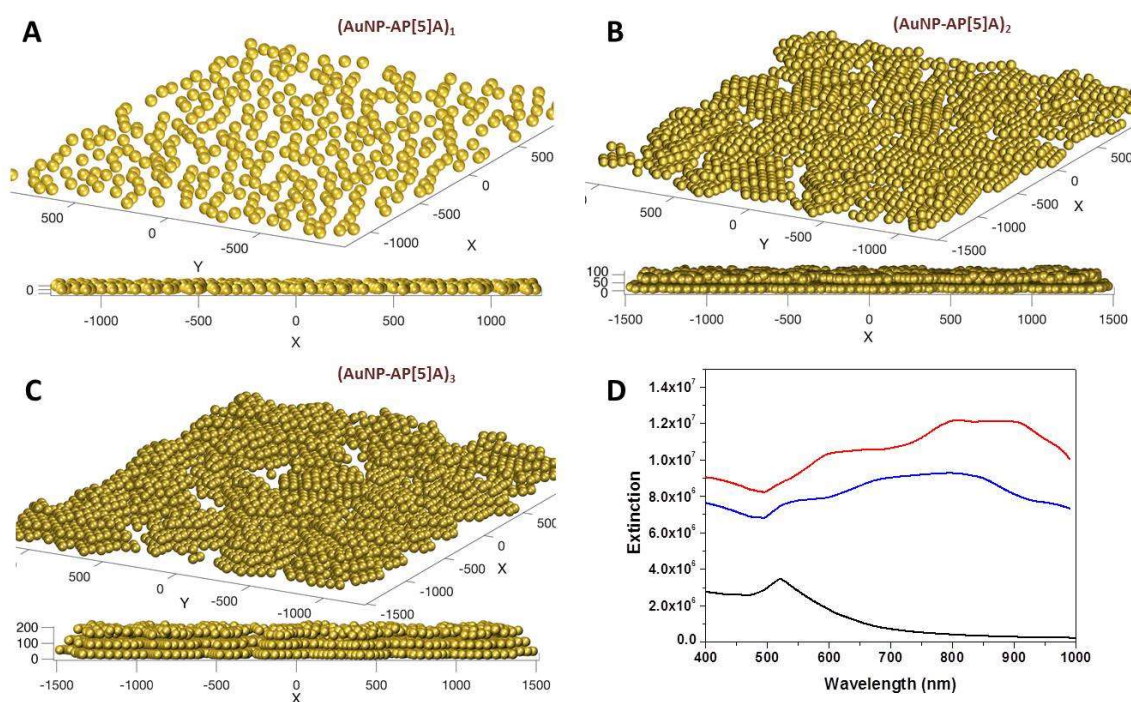


Figure S6. (A-C) Computer aided design (CAD) models of the different AuNP-AP[5]A assemblies employed for the simulation of extinction: (A) $(\text{AuNP-AP[5]A})_1$, (B) $(\text{AuNP-AP[5]A})_2$ and (C) $(\text{AuNP-AP[5]A})_3$. The models were generated with 366, 1274 and 2926 Au spheres of 60 nm in diameter for $(\text{AuNP-AP[5]A})_1$, $(\text{AuNP-AP[5]A})_2$ and $(\text{AuNP-AP[5]A})_3$, respectively. (D) Calculated extinction spectra obtained using the M^3 solver for $(\text{AuNP-AP[5]A})_1$ (black), $(\text{AuNP-AP[5]A})_2$ (blue) and $(\text{AuNP-AP[5]A})_3$ (red).

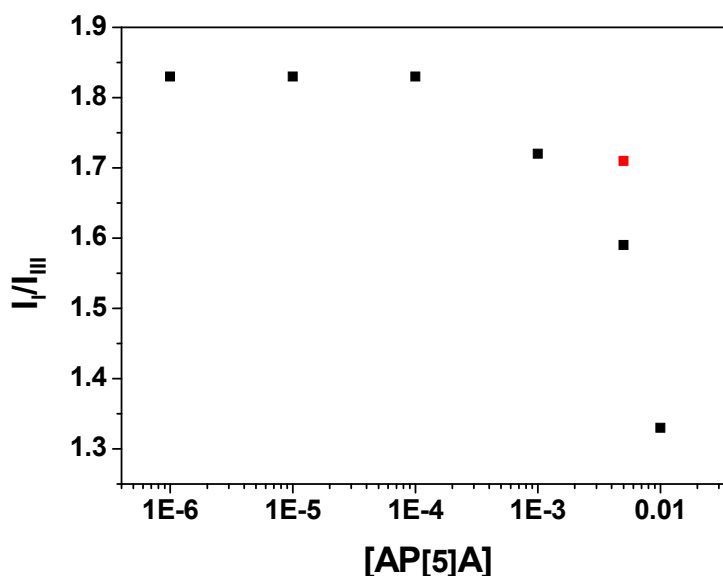


Figure S7. Band I:Band III intensity ratio (I_I/I_{III}) corresponding to 8×10^{-7} M pyrene as a function of the concentration of pillar[5]arene. The red point is the experimental value obtained when a competitive guest such as sodium toluenesulfonate (5×10^{-3} M) was added after the complexation of pyrene (8×10^{-7} M) with pillar[5]arene (5×10^{-3} M).

The host-guest interaction of macrocycles with guest molecules, such as PAH, is often analyzed by fluorescent spectroscopy. The emission of pyrene shows five mayor characteristic vibronic bands, Bands I, II, III, IV, V, at ~ 371 , 379 , 383 , 395 and 410 nm. Besides, it has been reported that Band I:Band III intensity ratio (I_I/I_{III}) is strongly dependent of the polarity of the surrounding medium.⁽¹⁾ This polarity dependence has been used to study the interaction between pyrene and cyclodextrins. Thus, the I_I/I_{III} decreases from 1.8 in water to 0.6 when pyrene formed a host:guest complex with two cyclodextrin units.^(2, 3) Based on that we have studied the host-guest complexation between pillar[5]arene and pyrene monitoring the evolution of the I_I/I_{III} of 8×10^{-7} M pyrene ($\lambda_{ex} = 334$ nm; $T = 25$ °C) with the concentration of pillar[5]arene. As shown in Figure S7 the I_I/I_{III} shows a remarkable decrease from 1.8 for pillar[5]arene concentrations higher than 10^{-4} M achieving a value of 1.2 for concentrations of 10^{-2} M. It is indicative of the host:guest interaction between the two entities. Finally, to the sample containing 8×10^{-7} M pyrene and 5×10^{-3} M pillar[5]arene (I_I/I_{III} of 1.59) we added a competitive guest, 5×10^{-3} M sodium toluenesulfonate, which produced an increase in the value to 1.71 (red point in Figure S7).

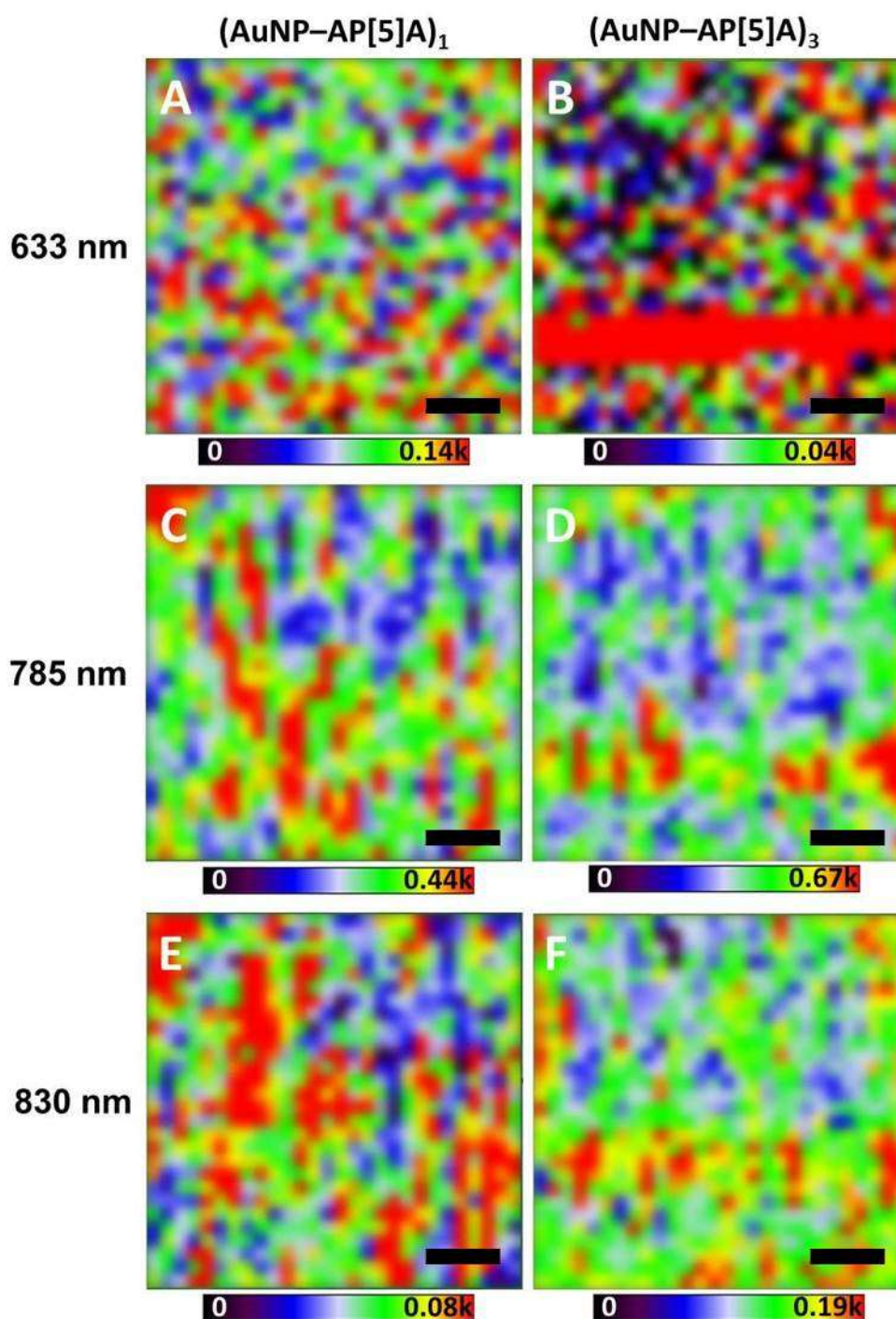


Figure S8. Representative SERS mappings obtained at 594 cm^{-1} for $(\text{AuNP-AP[5]A})_1$ (**A, C and E**) and $(\text{AuNP-AP[5]A})_3$ (**B, D and F**) with 633 nm (**A and B**), 785nm (**C and D**) and 830 nm (**E and F**) excitation laser lines. Pyrene concentration was $0.1\text{ }\mu\text{M}$. All SERS measurements were carried out with a 50 x objective and a maximum power of 43 kWcm^{-2} , 52 kWcm^{-2} and 11 kWcm^{-2} for the 633, 785 and 830 nm laser lines, respectively. The acquisition time was 1 s. All scale bars represent $20\text{ }\mu\text{m}$.

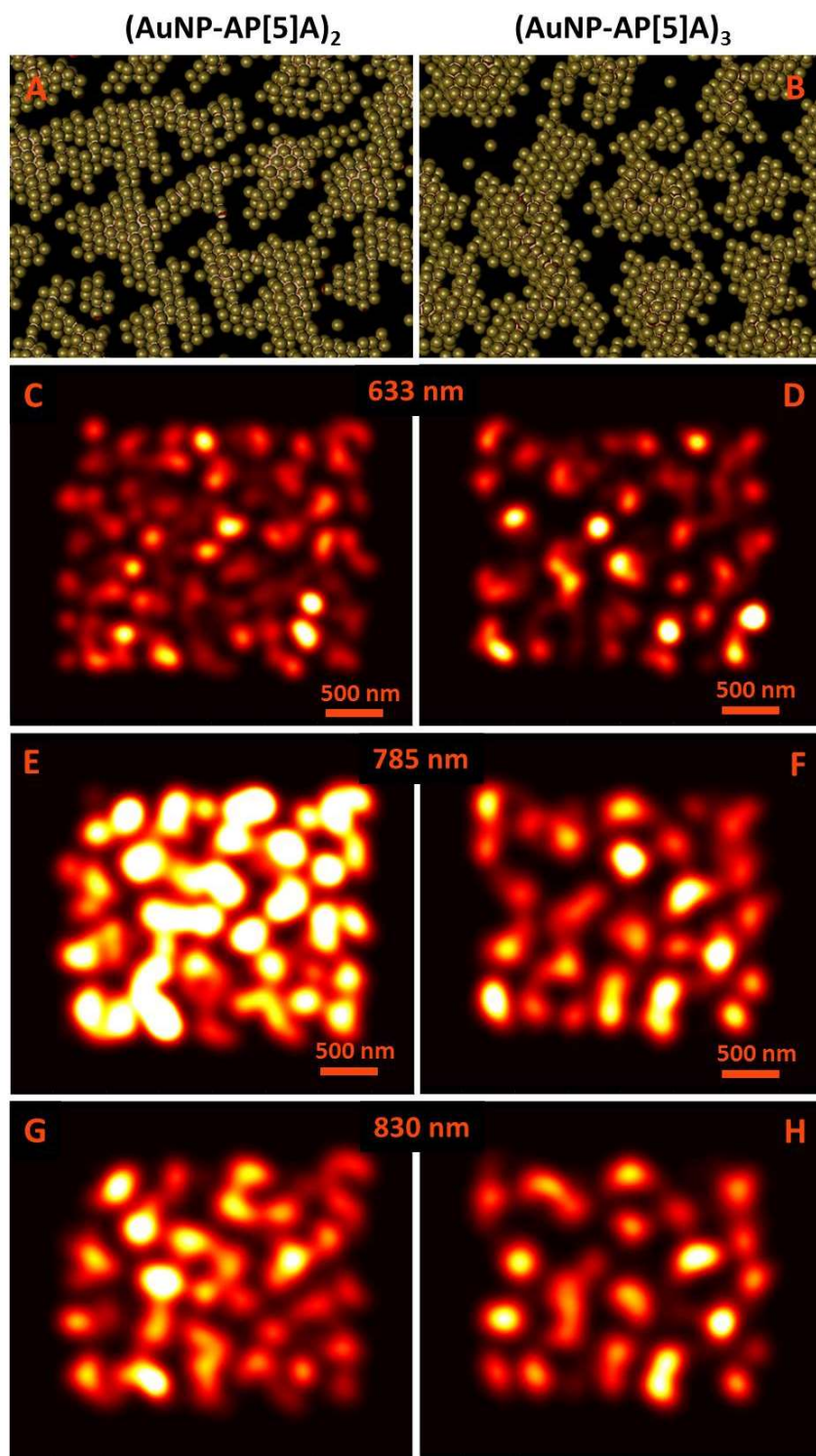


Figure S9. Simulated SERS mappings for $(\text{AuNP-AP[5]A})_2$ and $(\text{AuNP-AP[5]A})_3$ obtained with 633 nm, 785nm and 830 nm excitation wavelengths. SERS is calculated for zero Raman shift as $|E/E_{\text{inc}}|^4$. **(A-B)** Detailed geometry employed to obtain SERS on closed surfaces (skins) surrounding each nanoparticle, with a nanoparticle-to-molecule separation of 0.72 nm, consistent with the interparticle ligands. **(C-H)** Calculated SERS mappings depicting the weighted SERS for $(\text{AuNP-AP[5]A})_2$ (**C, E, G**) and $(\text{AuNP-AP[5]A})_3$ (**D, F, H**) and for the different excitation laser lines as indicated. The high-resolution SERS mappings are low-pass filtered through a Gaussian 2D profile with 0.1λ standard deviation (corresponding to N. A. = 0.75) to account for the lens diffraction, posing a more realistic picture.

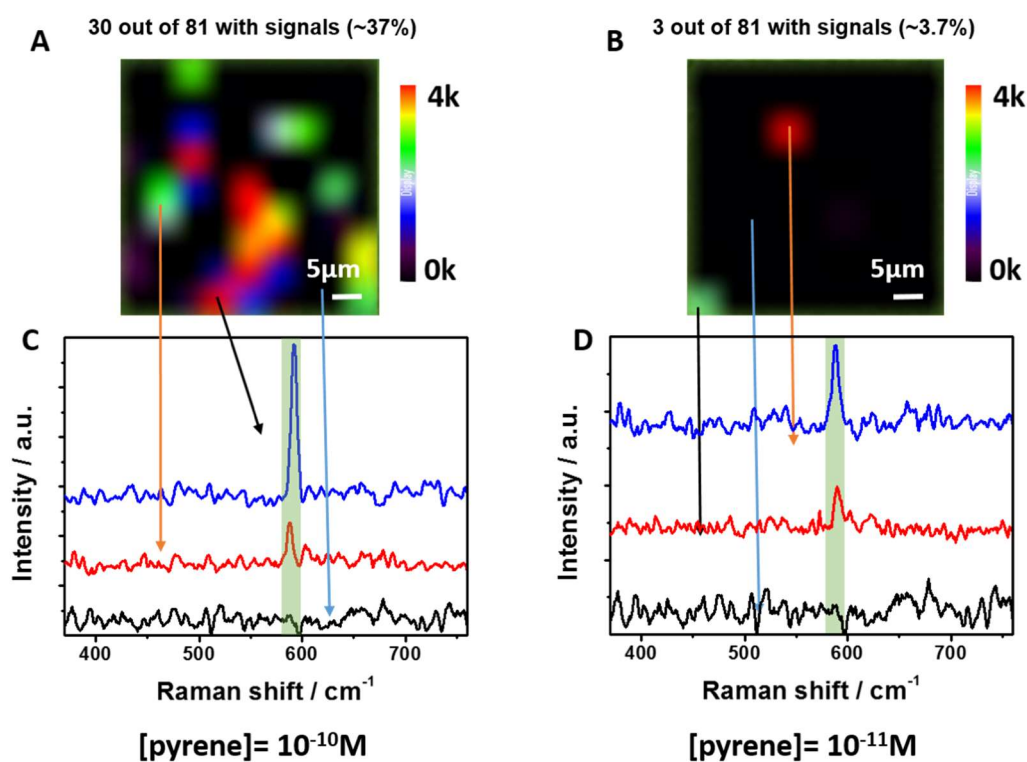


Figure S10. SERS mapping analysis of pyrene at 595 cm^{-1} from 10^{-10} M (A) and 10^{-11} M (B) aqueous solutions. (C-D) SERS spectra obtained from the marked sites in the mapping data. The SERS spectrum of the substrate has been subtracted for clarity.

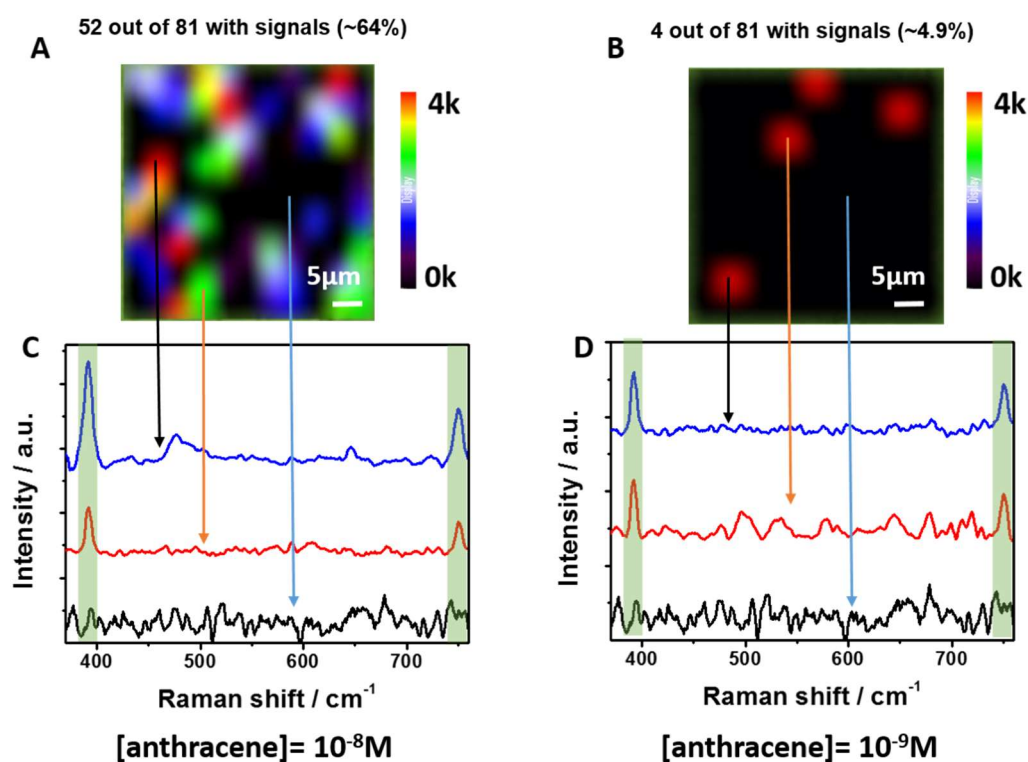


Figure S11. SERS mapping analysis of nitrophenyl at 633 cm^{-1} from 10^{-8} M (A) and 10^{-9} M (B) aqueous solutions. (C-D) SERS spectra obtained from the marked sites in the mapping data. The SERS spectrum of the substrate has been subtracted for clarity.

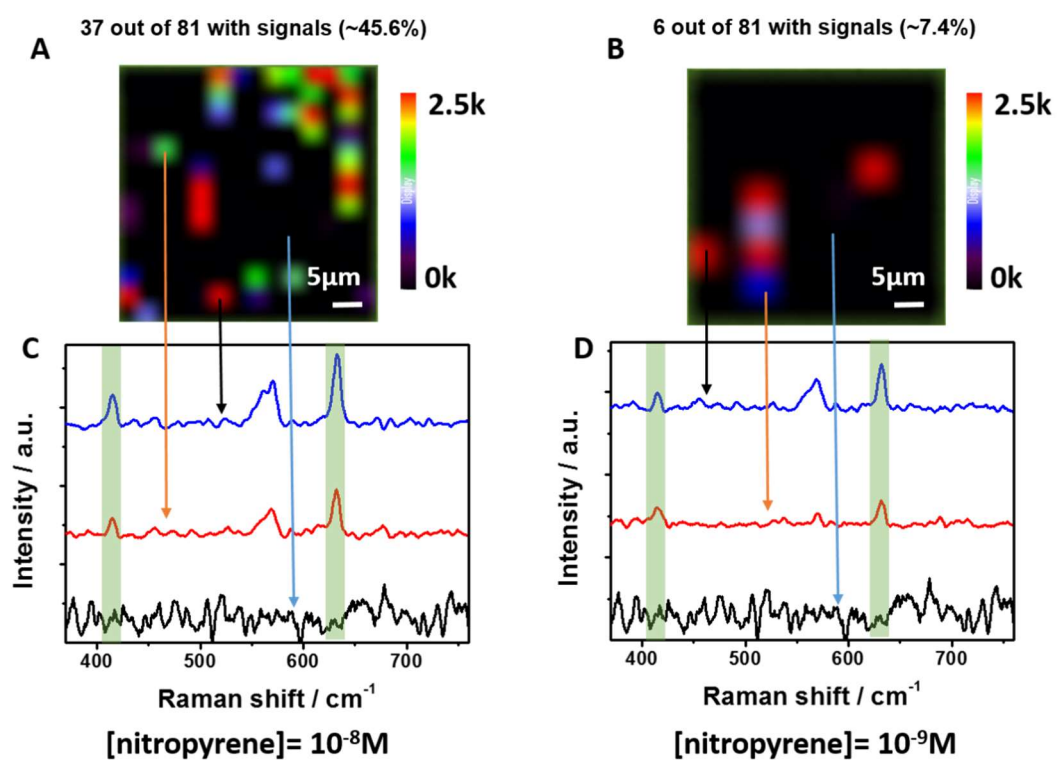


Figure S12. SERS mapping analysis of anthracene at 395 cm^{-1} from 10^{-8} M (**A**) and 10^{-9} M (**B**) aqueous solutions. (**C-D**) SERS spectra obtained from the marked sites in the mapping data. The SERS spectrum of the substrate has been subtracted for clarity.

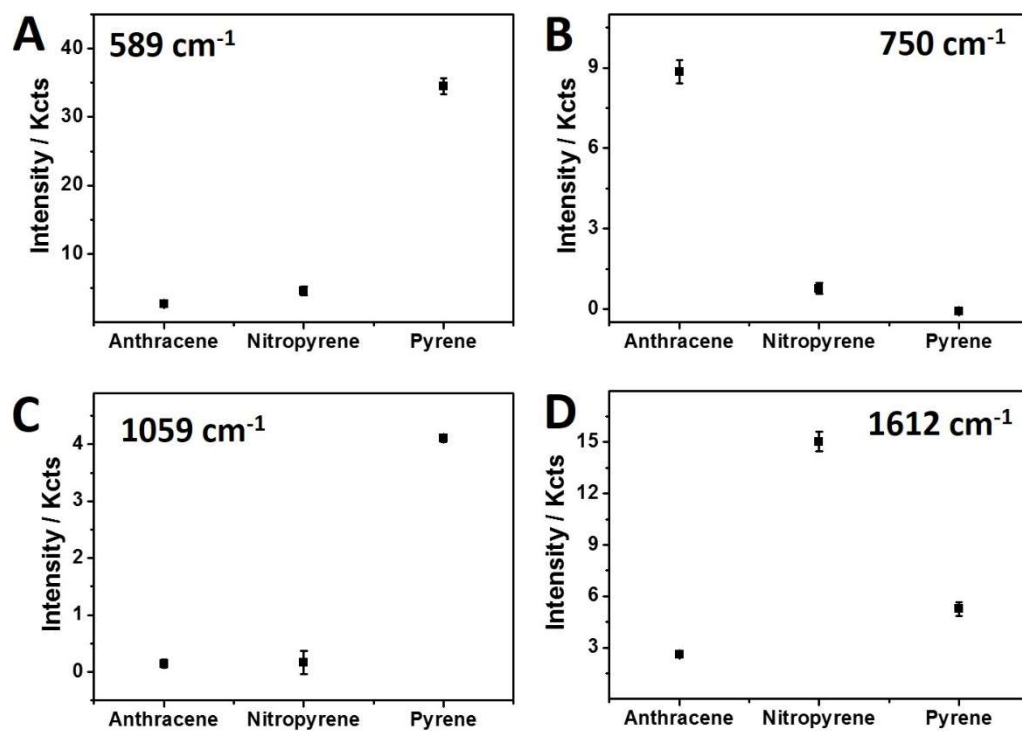


Figure S13. (A-D) Exploratory boxplots for the most relevant Raman shift 589 cm⁻¹ **(A)**, 750 cm⁻¹ **(B)** 1059 cm⁻¹ **(C)** and 1612 cm⁻¹ **(D)** to differentiate the three studied PAH in a mixture.

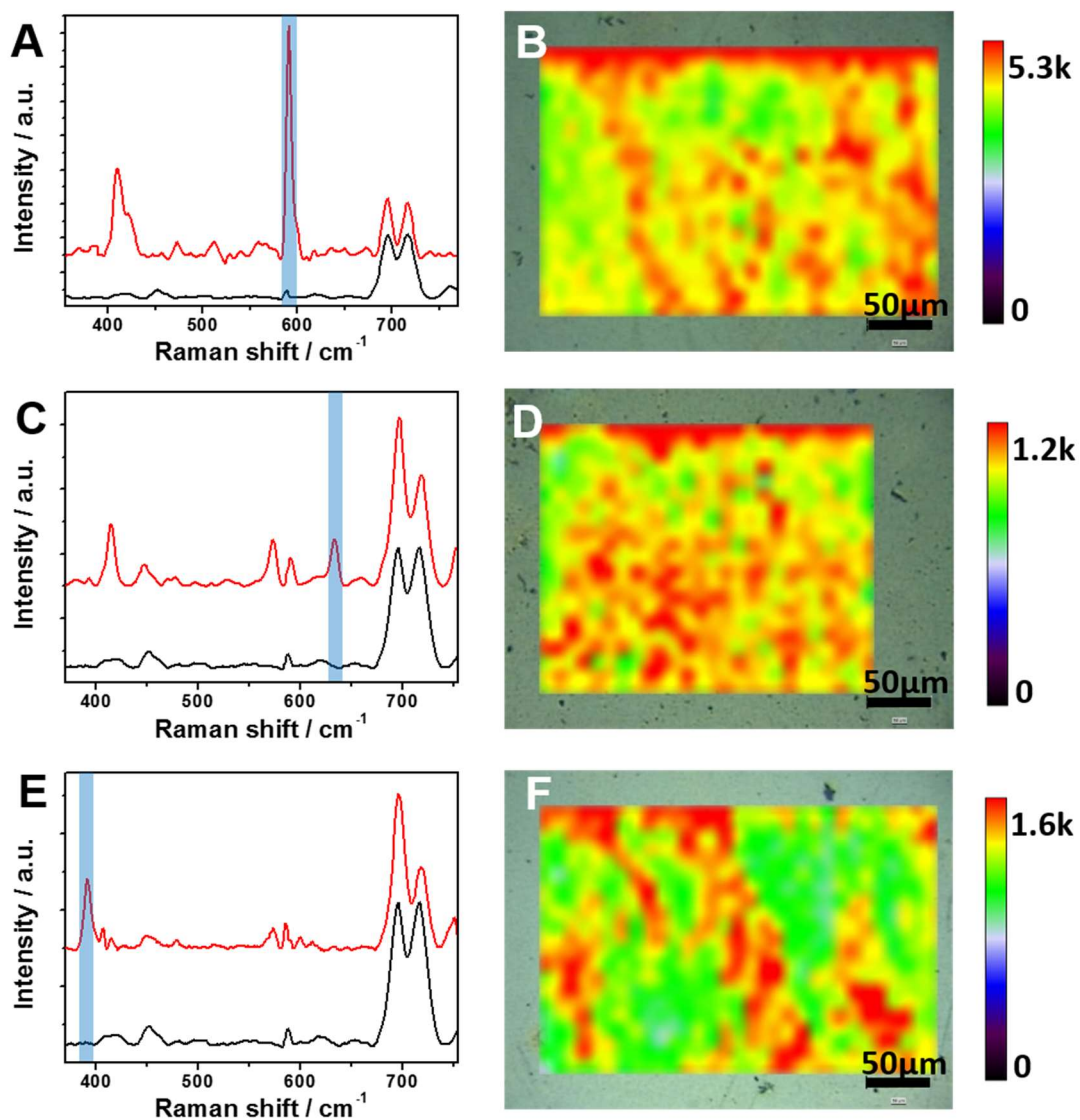


Figure S14. SERS spectra of pyrene (A), nitropyrene (C) and anthracene (E) obtained from gas-phase experiment. The SERS spectrum of the substrate has not been subtracted therefore it has been included in the graphs (black spectra). SERS intensity mappings of pyrene (B) at 594 cm^{-1} , nitropyrene (D) at 633 cm^{-1} , and anthracene (F) at 395 cm^{-1} . An excitation laser line at 785 nm was used for all measurements.

Table S1. Summary of the vibrational band assignments for pyrene, 1-nitropyrene and anthracene.

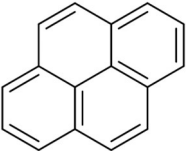
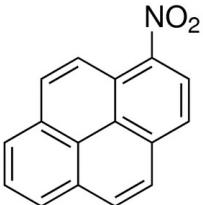
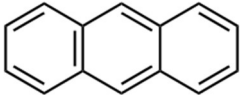
Pyrene		1-Nitropyrene		Anthracene	
					
Raman shift / cm^{-1}	Assignment	Raman shift / cm^{-1}	Assignment	Raman shift / cm^{-1}	Assignment
1614	Ring C=C stretching (4)	1614	C-C stretching (5, 6)	1661	
1401	Ring C=C stretching (4)	1404	C-C stretching (5)	1543	C-C stretching (7, 8)
1235	Ring C=C stretching (4,5)	1236	C-C stretching / C-H in-plane bending (5)	1393	Ring stretching (7)
1139	CH bending (4)	1151	C-H in-plane bending (5)	1175	C-C stretching (7)
1060	CH bending (4)	1036	C-H in-plane bending (5)	1154	C-C stretching (7)
590	Ring breathing (4)	633	NO ₂ in-plane bending (5) Ring breathing (6)	1031	
407	Ring deformation (4)	416	Skeletal stretching (5) Ring deformation (6)	1004	C-C stretching (7)
		357	Skeletal stretching (5) Ring deformation (6)	750	Stretching (7)
				479	Skeletal deformation (7)
				392	Skeletal deformation (7)

Table S2. Summary of SERS detection limits reported for the three PAH studied.

Detection platform	PAH/LOD	Reference
Au colloids	Pyrene/ 4.4×10^{-8} M Anthracene/ 1.8×10^{-9} M	(9)
Au NPs coupled film	Pyrene/ 6.3×10^{-8} M	(10)
Fe ₃ O ₄ @Au colloids	Pyrene/ 5.0×10^{-8} M Anthracene/ 5.0×10^{-8} M	(11)
Pillar[5]arene-functionalized Au colloids	Pyrene/ 1.0×10^{-8} M	(4)
Dithiocarbamate-functionalized Ag colloids	Pyrene/ 1.0×10^{-8} M	(12)
Au NPs on polymeric platforms	Pyrene/ 1.1×10^{-7} M Anthracene/ 0.93×10^{-7} M	(13)
Ag-doped filter paper	Nitropyrene/ 2.0×10^{-4} M	(14)
Silver cavities	Anthracene/ 8×10^{-9} M Pyrene/ 4×10^{-8}	(8)
Ag coated spheres on glass	Nitropyrene/ 10^{-6} M	(15)

References.

1. Kalyanasundaram, K.; Thomas, J. K. Environmental Effects on Vibronic Band Intensities in Pyrene Monomer Fluorescence and their Application in Studies of Micellar Systems. *J. Am. Chem. Soc.* **1977**, *99*, 2039-2044.
2. Muñoz de la Peña, A.; Ndou, T.; Zung, J. B.; Warner, I. M. Stoichiometry and Formation Constants of Pyrene Inclusion Complexes with Beta- and Gamma-Cyclodextrin. *J. Phys. Chem.* **1991**, *95*, 3330-3334.
3. Dyck, A. S. M.; Kisiel, U.; Bohne, C. Dynamics for the Assembly of Pyrene- γ -Cyclodextrin Host-Guest Complexes. *J. Phys. Chem. B* **2003**, *107*, 11652-11659, and references therein.
4. Montes-García, V.; Fernández-López, C.; Gómez, B.; Pérez-Juste, I.; García-Río, L.; Liz-Marzán, L. M.; Pérez-Juste, J.; Pastoriza-Santos, I. Pillar[5]Arene-Mediated Synthesis of Gold Nanoparticles: Size Control and Sensing Capabilities. *Chem. Eur. J.* **2014**, *20*, 8404-8409.
5. Carrasco, E. A.; Campos-Vallette, M.; Leyton, P.; Diaz G.; Clavijo, R. E.; García-Ramos J. V.; Inostroza N.; Domingo, C.; S. Sanchez-Cortes, S.; Koch, R. Study of the Interaction of Pollutant Nitro Polycyclic Aromatic Hydrocarbons with Different Metallic Surfaces by Surface-Enhanced Vibrational Spectroscopy (SERS and SEIR). *J. Phys. Chem. A* **2003**, *107*, 9611-9619.
6. Carrasco-Flores, E. A.; Clavijo, R. E.; Campos-Vallette, M. M.; Aroca R. F. Vibrational Spectra and Surface-Enhanced Vibrational Spectra of 1-Nitropyrene. *Appl. Spectrosc.* **2004**, *58*, 555-561.
7. Qu, L.-L.; Li, Y.-T.; Li, D.-W.; Xue, J.-Q.; Fossey, J. S.; Long, Y.-T. Humic acids-based one-step fabrication of SERS substrates for detection of polycyclic aromatic hydrocarbons. *Analyst* **2013**, *138*, 1523-1528.
8. Gu, X.; Tian, S.; Zhou, Q.; Adkins, J.; Gu, Z.; Li, X.; Zheng, J. SERS detection of polycyclic aromatic hydrocarbons on a bowl-shaped silver cavity substrate. *RSC Adv.* **2013**, *3*, 25989-25996.
9. Shi, X.; Liu, S.; Han, X.; Ma, J.; Jiang, Y.; Yu, G. High-Sensitivity Surface-Enhanced Raman Scattering (SERS) Substrate Based on a Gold Colloid Solution with a pH Change for Detection of Trace-Level Polycyclic Aromatic Hydrocarbons in Aqueous Solution. *Appl. Spectrosc.* **2015**, *69*, 574-579.
10. Gu, H. X.; Hu, K.; Li, D. W.; Long, Y. T. SERS detection of polycyclic aromatic hydrocarbons using a bare gold nanoparticles coupled film system. *Analyst* **2016**, *141*, 4359-4365.
11. Du, J. J.; Xu, J. W.; Sun, Z. L.; Jing, C. Y. Au nanoparticles grafted on Fe₃O₄ as effective SERS substrates for label-free detection of the 16 EPA priority polycyclic aromatic hydrocarbons. *Anal. Chim. Acta* **2016**, *915*, 81-89.
12. Guerrini, L.; Garcia-Ramos, J. V.; Domingo, C.; Sanchez-Cortes, S. Sensing Polycyclic Aromatic Hydrocarbons with Dithiocarbamate-Functionalized Ag Nanoparticles by Surface-Enhanced Raman Scattering. *Anal. Chem.* **2009**, *81*, 953-960.
13. Wang, X.; Hao, W.; Zhang, H.; Pan, Y.; Kang, Y.; Zhang, X.; Zou, M.; Tong, P.; Du, Y. Analysis of polycyclic aromatic hydrocarbons in water with gold nanoparticles decorated hydrophobic porous polymer as surface-enhanced Raman spectroscopy substrate. *Spectrochim. Acta Part A* **2015**, *139*, 214-221.
14. Laserna, J.J.; Campiglia, A.D.; Winefordner, J.D. Mixture Analysis and Quantitative-Determination of Nitrogen-Containing Organic-Molecules by Surface-Enhanced Raman Spectrometry. *Anal. Chem.* **1989**, *61*, 1697-1701.
15. Enlow, P. D.; Buncick, M.; Warmack, R. J.; Vo-Dinh, T. Detection of Nitro Polynuclear Aromatic-Compounds by Surface-Enhanced Raman-Spectrometry. *Anal. Chem.* **1986**, *58*, 1119-1123.